LETTERS TO THE EDITOR

The Letters to the Editor section is divided into four categories entitled Communications, Notes, Comments, and Errata. Communications are limited to three and one half journal pages, and Notes, Comments, and Errata are limited to one and three-fourths journal pages as described in the Announcement in the 1 January 1994 issue.

COMMUNICATIONS

Detection of the perpendicular $\tilde{A}$ state transitions of CH_3I by imaging of photofragment angle-velocity distributions

Robert A. Hertz and Jack A. Syage
The Aerospace Corporation, P. O. Box 92957/M5-754, Los Angeles, California 90009

(Received 17 February 1994; accepted 8 April 1994)

Photofragment angle-velocity distributions are measured in a molecular beam using a new two-dimensional imaging technique. We report on the detection of weak perpendicular transitions for CH_3I $\tilde{A}$ state photodissociation at 266 and 304 nm. The ratio of cross sections and the $^3Q_0-{}^1Q$ crossing probability are $\sigma_\perp/\sigma_\parallel=0.00-0.10$ and $p=0.22-0.27$ at 266 nm and $\sigma_\perp/\sigma_\parallel=0.20-0.30$ and $p=0.43-0.48$ at 304 nm.

The photodissociation of CH_3I has become a benchmark for testing theories and computational methods of calculating potential energy surfaces of polyatomic molecules. The $\tilde{A}$ states undergo direct dissociation to CH_3 and I.[1–6] Photofragment anisotropy measurements indicate that I atoms formed in both the $^2P_{3/2}$ and $^2P_{1/2}$ spin–orbit states originate from an $\tilde{A}\leftarrow\tilde{X}$ transition of CH_3I involving a parallel transition moment, even though the $I(^2P_{3/2})$ ground state correlates to a perpendicular transition.[1–5] These observations are explained by a dominant parallel transition to a potential surface that correlates with $I(^2P_{1/2})$ [henceforth I*], but which undergoes a branching at a surface crossing with a state that correlates with $I(^2P_{3/2})$ [henceforth I].

A crucial issue that remains unresolved is the relative contribution to the perpendicular states from direct excitation versus from surface crossing. The detection of weak perpendicular transitions that are overlapped by a strong parallel band is achieved here by a new photofragment imaging technique that records two-dimensional images of the three-dimensional velocity distribution in the form of 2D "slices" rather than projections that must be inverted. In this Communication we measure the ratio of parallel and perpendicular transition cross sections, which in combination with measurements of the branching ratio to I and I* permits the surface crossing probability to be determined as a function of photolysis wavelength.

Background: The $\tilde{A}$ states of CH_3I are due to $5pn\rightarrow\sigma^*$ excitations that are split by spin–orbit interactions into five components. Transitions to three component states are electric-dipole allowed from the ground electronic state and are denoted in order of increasing energy as $^3Q_1$, $^3Q_0$, and ^1Q (Mulliken notation, $2E$, $2A_1$, and $3E$ in C_{3v} symmetry).[7] The $^3Q_1$ and ^1Q states are reached by transition moments perpendicular to the C–I bond and the $^3Q_0$ state by a parallel transition moment. The perpendicular transitions correlate to the $CH_3+I(^2P_{3/2})$ dissociative limit and the parallel transition correlates to the $CH_3+I^*(^2P_{1/2})$ limit.[7–9] These simple considerations predict a crossing of the $^3Q_0$ and ^1Q surfaces.

The angular distribution of photofragments (expressed as a differential cross section) is given by

$$\frac{d\sigma}{d\Omega}=\frac{\sigma}{4\pi}\left[1+\frac{\beta}{2}(3\cos^2\theta-1)\right], \tag{1}$$

where θ is the fragment ejection angle relative to the laser polarization axis, σ is the integral absorption cross section, and β is the anisotropy parameter, which in the limit of direct dissociation is -1 or $+2$ for perpendicular and parallel transitions, respectively. In the diabatic picture of the $\tilde{A}$ state potentials, one would expect I and I* to be produced with angular distributions corresponding to β values of -1 and 2, respectively (i.e., angular distributions peaking perpendicular to and parallel to the laser polarization axis, respectively). Instead, photofragment anisotropy measurements show that both I and I* exhibit parallel-like dissociation.[1–5] These results are explained by a dominant parallel transition to $^3Q_0$ that undergoes a branching at the $^3Q_0-{}^1Q$ surface crossing to give both I and I*. Calculations support this interpretation.[8,9] Butler and co-workers presented convincing experimental evidence for the surface crossing and branching by showing that the emission polarization from $\tilde{A}$ state excitation evolves from a pure parallel component to a mixture of parallel and perpendicular components.[10]

Experimental: The method of recording 2D images of 3D angle-velocity distributions is illustrated in Fig. 1. Photodissociation is initiated and products subsequently ionized by laser excitation. The expanding ion packet (shown as a sphere in Fig. 1 for clarity) represents the 3D angle-velocity distribution. A series of time-of-flight spectra are collected using a rastering procedure in which the position of the ionized photoproduct packet is stepped across the detector aperture by incrementing the voltage across a pair of deflector plates.

The velocity components in a specific plane of interest are dispersed temporally along the z-axis and spatially along either the x or y axis. The c.m. velocity components in the laboratory axis system are given by the relations

 0021-9606/94/100(12)/9265/4/$6.00

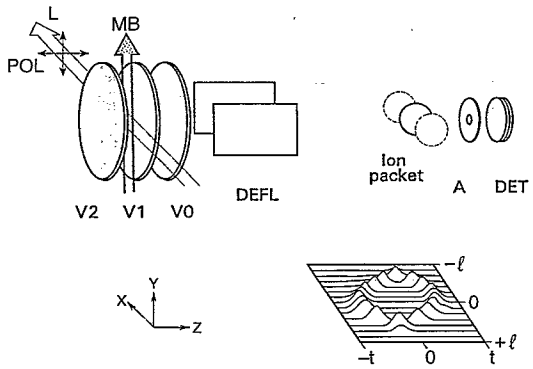

FIG. 1. Time-of-flight ion optics assembly used for measuring photofragment angle-velocity distributions (not to scale). Terms are defined as follows: A, aperture; DEFL, ion deflector plates; DET, detector; L, laser, MB, molecular beam; POL, laser polarization axis; V0, V1, V2, ion acceleration grids. Deflector plates for y axis are not shown. A simulated spectrum is illustrated for the xz plane.

$$v_z = \frac{q\epsilon(t_0 - t)}{m}, \tag{2}$$

$$v_{x,y} = \frac{l}{t_0} = \frac{1}{t_0}(KV_{\mathrm{DEFL}}). \tag{3}$$

Equation (2) assumes two-stage ion acceleration under space focussing conditions where ϵ is the extraction field, q is charge, m is mass, and $t - t_0$ is the arrival time relative to the center of the distribution t_0.[11] In Eq. (3), K is a constant relating the deflection voltage V_{DEFL} to the spatial deflection l at the detector. Our time-of-flight mass spectrometer consists of an ion optics assembly of three grids V0–V2 each separated by 1 cm, a 1 m drift tube, and a 5 mm diam aperture mounted in front of an 18 mm diam microchannel plate detector. The results presented here were collected using 15 V/cm and 230 V/cm for the extraction and acceleration fields, respectively. Under these operating conditions, I^+ ions have flight times centered at $t_0 = 72$ μs. A combination of the detector aperture diameter and blurring of the ion image due to diffraction off grids currently limits our spatial resolution to about 8 mm giving a best angular resolution of about $\pm 6°$ for the highest velocity I atom fragments.

Photofragment images can be recorded in the xz and yz planes depending on whether the x or y deflector plates are used. The laser polarization axis P is aligned along either the z axis or y axis (denoted P_z and P_y). We define the c.m. velocity components parallel and perpendicular to P as w and u,v, respectively. The xyz laboratory axis system, therefore, corresponds to the c.m. velocity components uvw and uwv for P_z and P_y polarization, respectively. Hence, the xz and yz laboratory planes yield three orthogonal and one redundant c.m. planes of detection: uw and vw (for P_z) and uv and wv (for P_y).

Photolysis was initiated at 266 nm or 304 nm. I and I* photofragment were ionized by 2+1 resonance enhanced multiphoton ionization (REMPI) using excitation at 304.7 nm ($6P^2D^0_{5/2}$ intermediate state) and 304.0 nm ($6P^4D^0_{1/2}$ state), respectively. Laser pulse energies and focussing conditions were adjusted to avoid space charge repulsion and in the case of 266-nm photolysis to maximize the two-pulse signal relative to the one-color signal. TOF spectra were collected using a LeCroy 9450 digital scope. The images reported here required about 30 minutes of data acquisition time at 10-Hz laser operation.

The CH_3I sample was placed in a bubbler cooled to 0 °C and delivered to the pulsed valve by a flow of Ar or He at 400 psi (results were unchanged at lower temperatures). To inhibit cluster excitation, the pulsed valve was heated to 60 °C and excitation was synchronized to the leading edge of the gas pulse. Cluster formation was negligible under these conditions as verified by low energy electron impact mass spectra and corroborated in the angle-velocity images by the absence of the characteristic low energy I atoms from cluster photodissociation.[3]

The present technique has important similarities and differences to previous methods that use time-of-flight mass spectrometry (TOF/MS) to measure fragment velocity. The groups of Houston,[3] El-Sayed,[12] and Chandler[13] have obtained TOF velocity distributions along one axis of the 3D distribution (Houston refers to it as core sampling). Measurements along two axes were obtained by rotating the laser polarization. These measurements use delayed ion extraction to achieve large separation of the velocity components, but the lack of space focussing conditions complicate the relationship between v and $t - t_0$. The groups of Crim and Powis operated under space focussing conditions, but recorded 1D projections rather than 1D cores by foregoing the use of an aperture at the detector (i.e., the entire ion packet was intercepted by the detector).[4] Houston and Chandler developed a TOF/MS imaging technique by impinging the ion packet onto an intensified microchannel plate camera system.[5] These 2D images are projections that require an Abel inversion to obtain images in a single plane from which speed distributions are obtained. The inversion routine, however, can introduce aberrations in the processed data. Doppler selection has been used to record 2D slices by ion imaging (Kinugawa and Arikawa) and by fluorescence imaging (Chen).[14] These methods work best for fast, and therefore, light fragments. The method of photofragment translational energy spectroscopy using a rotating detector yields angle-velocity distributions in a single plane, but in the laboratory frame.[1,2] Transformation to the c.m. frame requires an interative forward convolution routine. The advantage of the present method is that no reconstruction of data is required to obtain in-plane c.m. angle-velocity distributions.

Results: For axisymmetric systems only two planes of detection are needed. We choose the xz laboratory frame, which corresponds to the uw and uv velocity planes for P_z and P_y, respectively. The product angular distributions expected for directly dissociating parallel and perpendicular transitions ($\beta = 2$ and -1, respectively) are illustrated in Fig. 2. The 1D projections of the 2D images are also shown. *The uv plane is especially important because it probes in the node of the parallel angular distribution and, therefore, is very sensitive to detecting perpendicular transitions.*

The uw and uv image planes were recorded for I and I*

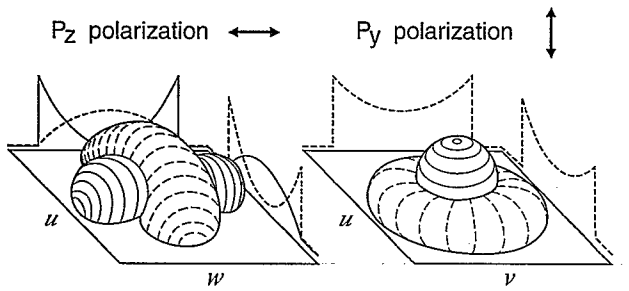

FIG. 2. Representation of the angular probabilities for photofragment ejection angle arising from parallel (—) and perpendicular (- - -) transitions of CH_3I in two planes of detection that selectively probe these two transitions. u, v, and w are orthogonal c.m. velocity components. The plane of detection was varied in this example by rotating laser polarization P. 1D projections of the intensity profiles of the 2D velocity images are calculated along the edges.

for 266 and 304 nm photolysis. The results for 304 nm photolysis and I atom probe are shown in Fig. 3. A strong forward-backward peaked angular distribution is observed in Fig. 3(a) for the uw plane, corresponding to the direct dissociation from a dominant parallel transition. The uv plane in Fig. 3(b), on the other hand, shows the characteristic "donut" shaped angular distribution expected for a perpendicular transition. Individual high sensitivity TOF spectra were also recorded along the image centerline at $u=0$. These spectra correspond to scattering through angles of $\theta=0°$ [$I_\parallel(w)$ trace] and $\theta=90°$ [$I_\perp(v)$ trace]. For I($^2P_{3/2}$) detection, the ratio of intensity $I_\perp/I_\parallel$ is 0.00–0.05 at 266 nm and 0.10–0.15 at 304 nm. Because of the limited angular resolution of the experiment (cf. Experimental), about 5–6 % of photofragments from parallel excitation, those with near orthogonal scattering angles, appear in the $I_\perp$ traces, and are subtracted out. The ratio $I_\perp/I_\parallel$ was much less for I* than for I, as expected since I* correlates with the strong parallel $^3Q_0$ state.

Discussion: The ratio of cross sections for perpendicular and parallel transitions is straightforward to determine. Equation (1) leads to the simple expression $\sigma_\perp/\sigma_\parallel=2I_\perp/I_\parallel$. Our measurements for I($^2P_{3/2}$) lead to $\sigma_\perp/\sigma_\parallel$ ratios of 0.00–0.10 at 266 nm and 0.20–0.30 at 304 nm. Gedanken and Rowe recorded absorption and magnetic circular dichroism (MCD) spectra of CH_3I, from which they determined the $^3Q_1$, $^3Q_0$, and ^1Q component contributions to the continuum $\tilde{A}$ band absorption.[15] The peak component absorption wavelengths are reported to be 300, 261, and 240 nm, respectively, and the percentage total absorption strengths are 1:78:21, respectively. The MCD results indicate a minimum in $\sigma_\perp/\sigma_\parallel$ at 260 nm, which is consistent with our results. At 304 nm the ratio of the weak $^3Q_1$ band to the far wing of the strong $^3Q_0$ band is difficult to access from the MCD results.

The surface crossing probability p can be determined from measurements of $\sigma_\perp/\sigma_\parallel$ and the branching ratio $f(\mathrm{I})/f(\mathrm{I}^*)$. Product yield can be expressed by

$$\begin{pmatrix} f(I) \\ f(I^*) \end{pmatrix} = \begin{pmatrix} 1-p & p & 1 \\ p & 1-p & 0 \end{pmatrix} \cdot \begin{pmatrix} \sigma_\perp(^1Q) \\ \sigma_\parallel(^3Q_0) \\ \sigma_\perp(^3Q_1) \end{pmatrix} \tag{4}$$

where we assume a crossing probability for the ^1Q and $^3Q_0$ surfaces, but not for the $^3Q_1$ surface, which lies at lower energy. The analysis simplifies considerably by assuming, based on theory[8] and MCD spectra,[15] that $\sigma_\perp(^1Q)\gg\sigma_\perp(^3Q_1)$ at 266 nm and $\sigma_\perp(^1Q)\ll\sigma_\perp(^3Q_1)$ at 304 nm. A value of $f(\mathrm{I})/f(\mathrm{I}^*)=0.37$ at 266 nm has been measured previously,[16] which in combination with the measured cross section ratio $\sigma_\perp/\sigma_\parallel=0.00$–$0.10$ yields a value for the crossing probability p of 0.22–0.27. At 304 nm, we estimate a

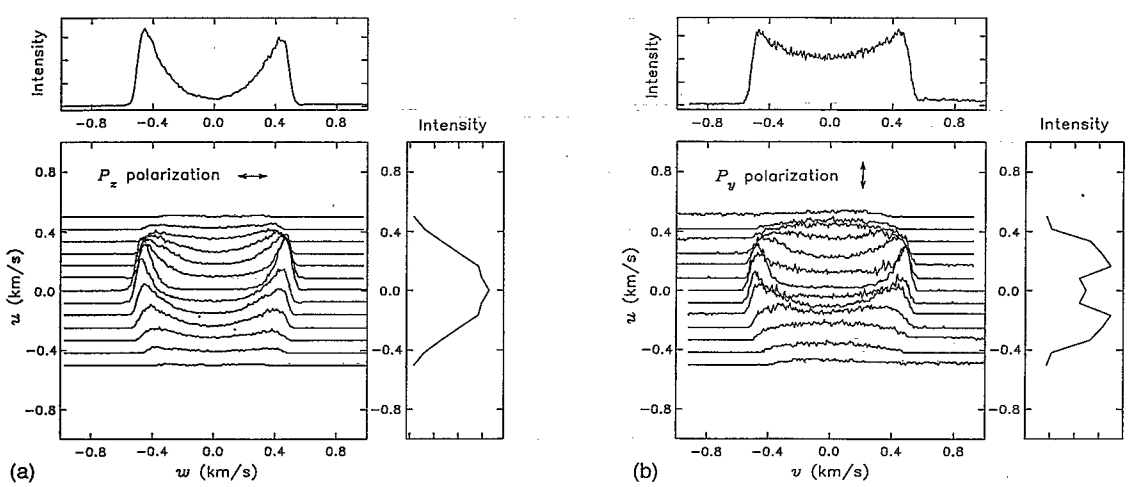

FIG. 3. Measurements of the 2D angle-velocity images of the I($^2P_{3/2}$) atom fragment from photodissociation of CH_3I at 304 nm. Shown are images in planes that selectively probe the (a) parallel and (b) perpendicular transitions. The intensity axis of the 2D images is out-of-plane and unlabeled. The 1D projections are obtained by summing the TOF spectra along each axis (compare to Fig. 2). Because the 3D distribution has a center of symmetry, we only recorded spectra for $u\geq0$. For visual clarity an inverted mirror image of this data is shown for $u<0$.

value of $f(I)/f(I^*)=1.3$ by scaling the branching ratio at 266 nm by the relative signal intensities of I and I* at the two wavelengths. An early photoacoustic study reports a value of about 2.0.[17] Using our branching ratio and cross section ratio of 0.20–0.30 yields a crossing probability of 0.43–0.48 at 304 nm.

Shapiro calculated crossing probabilities from the parallel transition of about 0.32 and 0.50 for 266 and 304 nm, respectively.[8] Although larger than the observed values, they exhibit the trend observed here that p increases with decreasing energy. Shapiro attributes this effect to the energy released into translation; the less translational energy, the slower is the passage through the crossing region, and consequently, the greater is the crossing probability.

In summary, the principal result here is the demonstration of a new photofragment imaging technique that delivers direct 2D c.m. images in the form of slices (as opposed to projections) of 3D velocity distributions. We have confirmed the existence of the weak ^1Q and $^3Q_1$ perpendicular transitions that overlap with the strong $^3Q_0$ parallel transition that make up the $\tilde{A}$ state continuum and determined relative cross sections and curve crossing probabilities at 266 and 304 nm.

[1] R. K. Sparks, K. Shobatake, L. R. Carlson, and Y. T. Lee, J. Chem. Phys. **75**, 3838 (1981).
[2] G. N. A. van Veen, T. Baller, A. E. de Vries, and N. J. A. van Veen, Chem. Phys. **87**, 405 (1984); M. D. Barry and P. A. Gorry, Mol. Phys. **52**, 461 (1984).
[3] R. Ogorzalek Loo, H.-P. Haerri, G. E. Hall, and P. L. Houston, J. Chem. Phys. **90**, 4222 (1989); R. Ogorzalek Loo, G. E. Hall, H.-P. Haerri, and P. L. Houston, J. Phys. Chem. **92**, 5 (1988).
[4] S. M. Penn, C. C. Hayden, K. J. Carlson Muyskens, and F. F. Crim, J. Chem. Phys. **89**, 2909 (1988); J. F. Black and I. Powis, Chem. Phys. **125**, 375 (1988).
[5] D. W. Chandler and P. L. Houston, J. Chem. Phys. **87**, 1445 (1987); D. W. Chandler, J. W. Thoman, Jr., M. H. M. Janssen, and D. H. Parker, Chem. Phys. Lett. **156**, 151 (1989).
[6] J. L. Knee, L. R. Khundkar, and A. H. Zewail, J. Chem. Phys. **83**, 1996 (1985).
[7] R. S. Mulliken, J. Chem. Phys. **8**, 382 (1940); *ibid.* **3**, 513 (1935).
[8] M. Shapiro, J. Phys. Chem. **90**, 3644 (1986).
[9] M. Tadjeddine, J. P. Flament, and C. Teichteil, Chem. Phys. **118**, 45 (1987); S. K. Gray and M. S. Child, Mol. Phys. **51**, 189 (1984).
[10] K. Q. Lao, M. D. Person, P. Xayariboun, and L. J. Butler, J. Chem. Phys. **92**, 823 (1990).
[11] J. L. Franklin, P. M. Hierl, and D. A. Whan, J. Chem. Phys. **47**, 3148 (1967).
[12] H. J. Hwang and M. A. El-Sayed, J. Phys. Chem. **96**, 8728 (1992); H. J. Hwang and M. A. El-Sayed, J. Chem. Phys. **94**, 4877 (1991).
[13] T. A. Spiglanin and D. W. Chandler, Chem. Phys. Lett. **141**, 428 (1987).
[14] T. Kinugawa and T. Arikawa, J. Chem. Phys. **96**, 4801 (1992); K-m. Chen, Chem. Phys. Lett. **198**, 288 (1992).
[15] A. Gedanken and M. D. Rowe, Chem. Phys. Lett. **34**, 39 (1975); *ibid.* **137**, 462 (1987).
[16] S. J. Riley and K. R. Wilson, Faraday Discuss. Chem. Soc. **53**, 132 (1972); W. P. Hess, S. J. Kohler, H. K. Haugen, and S. R. Leone, J. Chem. Phys. **84**, 2143 (1986).
[17] T. F. Hunter and K. S. Kristjansson, Chem. Phys. Lett. **58**, 291 (1978).